Enhancing the activity of biocatalysts supported on calcium phosphate by inducing mesoporosity with phosphopeptides

Surender Kumar Dhayal, Martin Lund, J M van den Brink, Ghouti Medjahdi, Alain Celzard, Vanessa Fierro, Carole Gardiennet, Andreea Pasc, Nadia Canilho

Enhancing the activity of biocatalysts supported on calcium phosphate by inducing mesoporosity with phosphopeptides

Surender Kumar Dhayal[a] dksudh@chr-hansen.com

Martin Lund[a] DKMTL@chr-hansen.com

J. M. van den Brink[a] DKHVB@chr-hansen.com

Ghouti Medjahdi[b] ghouti.medjahdi@univ-lorraine.fr

Alain Celzard[c] alain.celzard@univ-lorraine.fr

Vanessa Fierro[c] Vanessa.Fierro@univ-lorraine.fr

Carole Gardiennet[d] carole.gardiennet@univ-lorraine.fr

Andreea Pasc[e] andreea.pasc@univ-lorraine.fr

Nadia Canilho*[e] nadia.canilho@univ-lorraine.fr ; Phone number 00 33 3 72 74 54 98

[a] Chr. Hansen A/S, Boege Alle 10-12, 2970 Hoersholm, Denmark

[b] Université de Lorraine, CNRS, IJL, F-54000 NANCY, France

[c] Universtié de Lorraine, CNRS, F-88000 Epinal, France

[d] CRM2 UMR 7036 CNRS-Université de Lorraine, Bvd. des Aiguillettes, BP 70239, Vandoeuvre-lès-Nancy F-54506, France

[e] L2CM UMR 7053 CNRS-Université de Lorraine, Bvd. des Aiguillettes, BP 70239, Vandoeuvre-lès-Nancy F54506, France

*Corresponding authors

ABSTRACT

Preventing enzyme deactivation while increasing their accessibility by adsorption in mesopores remains a key challenge in the design of biocompatible supported enzymatic catalysts. Herein, it is expected that food-grade monomeric or polymeric glycopeptides containing organic phosphate groups (as casein phosphopeptide derivatives) enhances the entrapment of the enzyme over the one pot method of wet precipitation of calcium phosphate (CaP) leading to a biocompatible hybrid organic/inorganic catalyst.

The supported catalyst was prepared by wet precipitation of calcium and phosphorous in the presence of either monomeric glycopeptide or polymeric glycopeptide. These organic glycopeptides had an influence on the electrostatic stabilization during the nucleation of calcium phosphate particles, as tracked by dynamic light scattering and by scanning electron microscopy.

The phosphopeptide derivatives, were able to decrease the crystallization degree in calcium phosphate particles, as demonstrated by XRD and solid-state NMR analysis. Furthermore, according to N_2 sorption data, the glycopeptide derivatives induced interparticle mesopores, which might be responsible of the enhanced enzymatic activity of the supported biocatalyst that improved from 52 (+/-19) $NLU \cdot g^{-1}$ without organic compound to 607 (+/-34) $NLU \cdot g^{-1}$.

KEYWORDS : biomaterial; biomineralization; hydroxyapatite-like nanoparticles; enzymatic supported catalyst

1. Introduction

The wet precipitation of calcium and phosphate ions can lead to various calcium phosphate (CaP) polymorphs, including hydroxyapatite ($Ca_5(OH)(PO_4)_3H_2O$) [1]. The precipitation process starts with the nucleation and growth of primary particles, which can then aggregate into larger ones. Depending on the colloidal stability of the particles, inter-grains porosity can be induced, and in general, the higher is the stability, the higher is the porosity. Still, such particles exhibit only a low surface area and low pore volume, especially at the mesoscale, which limits the use of calcium phosphate support as a enzymatic biocatalyst. Strategies to tune the mesoporous texture in these inorganic particle matrices are based on controlling the crystal size and/or reducing the degree of crystallinity, either by using templates (e.g. based on self-assembled mesophases) to guide the crystal growth or by using polymeric coatings [2]. Much work on the immobilization of proteins on biocompatible supports such as porous silica for the development of enzymatic catalysts has also been published [3,4,5]. However, increasing the porosity of an inorganic support by coating it with organic food-grade polymers, for example, remains a straightforward approach compared to post-synthesis adsorption of the enzyme on a porous inorganic material. The coating strategy is much more suitable for bio-applications, especially for the elaboration of supported enzymatic catalysts. Indeed, both trapping and coating can be done *in situ* during the precipitation process of the inorganic matrix. Moreover, it is known that nucleation, growth and crystallinity of inorganic particles can be altered by the presence of a polymer in the synthesis medium [6,7]. The calcium phosphate nanoclusters (CaP) present in casein micelles are one example of particles stabilized by the organic phosphate groups of casein molecules. In general, casein adsorption is driven by interactions between the organic phosphate (serine-bound) and the surface of calcium phosphate particles. This adsorption

leads to a 'brush-like' layer of casein polymers that improves colloidal stability and prevents the aggregation of nanoclusters. Furthermore, it has reported that the crystalline degree of calcium phosphate particles can be attenuated by the presence of biomolecule containing organic phosphate during the precipitation reaction [8]. Moreover, when proteins such as enzymes will be involved together with organic phosphate in the precipitation reaction, its will be trapped in the pores of the inorganic matrix [9]. The size of most food-grade enzymes is in the range 2 – 20 nm, so the pore size of the inorganic matrix must be similar or slightly larger. Therefore, for the effective immobilization and retention of active molecules, both surface area and pore size must be controlled. In this study, we report the synthesis of supported biocatalysts by a one-step procedure involving wet precipitation and enzyme entrapment. An oligomeric or polymeric form of a phosphopeptide (*e.g.* casein glycomacropeptide or CGMP), extracted from whey, was added as a source of organic phosphate, to behave as a mesoporogen by modulating the crystallinity of the inorganic calcium phosphate matrix. The resulting materials were characterized in terms of porous texture, morphology and crystallinity. Additionally, DLS and ^{31}P NMR analysis were performed to better understand the formation mechanism of the hybrid inorganic-organic calcium phosphate particles. Finally, the catalytic efficiency of the biocatalyst support was determined as a function of the oligomer *vs* polymer nature of the glycopeptide.

2. Material and Methods

2.1 Materials

91 The casein glycomacropeptide (CGMP) was purified from a commercial sample (Lacprodan
92 CGMP-10, Arla Food Ingredients, Denmark) [10-13]. After purification, the dry matter
93 contained around 85 % protein of which about 73 % was monomeric CGMP (Mono-CGMP).
94 Polymeric CGMP (Poly-CGMP) was then prepared from this monomer by enzymatic
95 crosslinking with microbial transglutaminase (mTG), following a procedure previously
96 reported (see SI1) [14-18]. The enzyme (Enz), a lactase (Trade name Ha-Lactase, which
97 activity is of 5200 NLU·g^{-1} of solution, namely 100k NLU·g^{-1} of protein), was provided by Chr.
98 Hansen A/S, Denmark. The lactase activity was measured by using o-nitrophenyl-β-
99 galactopyranoside (ONPG) as substrate and the catalytic test was done according to the
100 method of Kim *et al*. [19]. The following chemicals were purchased either from Sigma
101 Aldrich for ONPG, dithiothreitol (DTT), calcium chloride dihydrate ($CaCl_2 \cdot 2H_2O$) and
102 magnesium sulphate heptahydrate ($MgSO_4 \cdot 7H_2O$)) or from Merck for disodium hydrogen
103 phosphate dihydrate ($Na_2HPO_4 \cdot 2H_2O$), sodium dihydrogen phosphate monohydrate
104 ($NaH_2PO_4 \cdot H_2O$), sodium chloride (NaCl), sodium carbonate (Na_2CO_3) and
105 ethylenediaminetetraacetic acid disodium salt dihydrate (EDTA). All were used as received.
106 The microbial transglutaminase (mTG) used for the enzymatic crosslinking of the monomeric
107 CGMP was from Ajinomoto and had an activity of 1000 U per g of powder, as measured by
108 the hydroxamate colorimetric method proposed by Folk *et al*. [20]. All other chemicals used
109 and mentioned in this work were of analytical grade.
110 The morphology and microstructure of the powdered microparticles were analysed using
111 Scanning Electron Microscopy (SEM, Hitachi microscope, Hitachi S4800). X-ray powder
112 diffraction analysis was performed at 45 kV and 40 mA, with a wavelength of $\lambda_{CuK\alpha}$= 1.5406
113 Å. The crystalline phases were identified by comparing the X-ray diffraction patterns with
114 the JCPDS powder diffraction files produced by the International Centre for Diffraction Data.

The degree of crystallinity (DOC) of the samples was calculated from the ratio between the total crystalline area divided by the sum of total crystalline area plus total amorphous area extracted from the diffusion background. Then, the amorphous content (%) was determined from 1-DOC (see SI6c). The molar ratio of calcium (Ca) to phosphate (P) was determined by ICP-OES elemental analysis.

2.2 Synthetic route: wet precipitation

Four materials have been synthesized by wet precipitation. The sample CaP refers to the pure inorganic matrix of calcium phosphate (CaP) prepared without enzyme (Enz) and CaP-Enz with enzyme. The hybrid particles obtained in the presence of enzyme and mono-CGMP (Mono) or poly-CGMP (Poly) have been abbreviated as CaP-Enz-Mono and CaP-Enz-Poly, respectively. The following stock solutions were used for preparing the different samples mentioned above: (a) 0.1 M sodium phosphate buffer and 0.1 M NaCl at pH 7.0, named Na-PB, (b), 4.5M $CaCl_2$, (c) 0.3M Na_2HPO_4, (d) 60 $g{\cdot}L^{-1}$ of Mono-CGMP in Na-PB, (e) 20 $g{\cdot}L^{-1}$ of Mono-CGMP in 0.3 M Na_2HPO_4, (f) 60 $g{\cdot}L^{-1}$ of Poly-CGMP in Na-PB, and (g) 20 $g{\cdot}L^{-1}$ of Poly-CGMP in 0.3 M Na_2HPO_4. The lactase enzyme stock solution (Enz) was used as received and MQ-water (W) was used in all stock solutions. The preparation of the different samples involved three sequential steps. Step-(i): Prepare 940 mL solution by mixing equal volumes of W and Na-PB (a) for CaP sample; Enz and Na-PB (a) for CaP-Enz sample; Enz and 60 $g{\cdot}L^{-1}$ of Mono-CGMP (d) for CaP-Enz-Mono sample; Enz and 60 $g{\cdot}L^{-1}$ of Poly-CGMP (f) for CaP-Enz-Poly sample. Step-(ii): 60 mL of $CaCl_2$ stock solution (b) were added dropwise for 5 min under 1000 rmp to 940 mL solution obtained in step-(i). Step-(iii): Addition of the resulting mixtures to 1L of respectively 0.3 M Na_2HPO_4 in the case of CaP and CaP-Enz samples, 20 $g{\cdot}L^{-1}$ of Mono-CGMP stock solution (e) for the CaP-Enz-Mono sample; and 20 $g{\cdot}L^{-1}$ of Poly-CGMP stock solution (g)

to prepare CaP-Enz-Poly. In each case the final pH was 7. Those solutions were also added over a period of 5 min under stirring at 1000 rpm. After additional 5 min of stirring, the mixtures were allowed to rest for 30 min and then were stirred at 500 rpm for 2 h at 20 °C. Mixing was stopped to allow particle sedimentation and slow growth and was continued gently after to avoid their agglomeration. At the end of step-(iii), the particle suspensions were centrifuged at 3000 × g (20 °C, 30 min). The pellets obtained after centrifugation were washed 3 times with 2L of MQ-water and dried at 20 °C using laminar airflow. The dried particles were hand grounded using a mortar and pestle and then stored in closed containers at room temperature. At the end of the step-(iii) 25 ± 3 g of dry powder was obtained from 1 L of starting suspension.

2.3 Loading and Activity of immobilized lactase

The amount of immobilized lactase in each sample was determined from sodium dodecyl sulphate-polyacrylamide gel electrophoresis (SDS-PAGE) and bicinchoninic acid (BCA) calibration curves (see SI2). The enzyme loading ($mg \cdot g^{-1}$) was calculated from the ratio of the measured amount of protein (mg) to the weight of dry powder (g). The average $mg \cdot g^{-1}$ of enzyme loading and standard deviation were obtained from three replicates. Briefly, the powdered catalyst was suspended in 1 mL of PEM buffer (the same as Britton-Robinson buffer, see SI3 for details) at 10 $g \cdot L^{-1}$. After separate incubation of catalyst and ONPG substrate solutions at 40 °C, the two preparations were mixed and stirred at 1000 rpm for 10 minutes at the same temperature of 40 °C. The reaction was then stopped by adding Na_2CO_3 (1M), followed by centrifugation at 10,000 × g for 5 minutes. The absorbance of the supernatant was measured at 420 nm. A blank measurement was done without any particles in the solution (see SI3). The measured activity was divided by the weight of the

dry powder to obtain the specific activity of the material, in $NLU \cdot g^{-1}$. The average $NLU \cdot g^{-1}$ and standard deviation were obtained from three replicates.

2.4 Textural characterization by nitrogen sorption

The BET area (A_{BET}) and the pore size distribution (PSD) were determined using nitrogen adsorption at -196°C in an automatic equipment (ASAP 2020, Micromeritics) [21-24]. All samples were pre-treated before nitrogen adsorption by degassing under secondary vacuum at 25 °C for at least 48h. The parameters of the analyses are detailed in SI4.

2.5 Dynamic Light Scattering (DLS) on colloidal CaP in the presence of Mono-CGMP or Poly-CGMP

The hydrodynamic radius (Rh) of the prepared colloidal CaP suspensions was measured at 25 °C using a Zetasizer (Nano ZSP, Malvern Instruments, Worcestershire, UK) equipped with a 633 nm laser. The intensity fluctuations in the scattered light were measured at 173° for 10 to 30 s. At least ten scans were averaged to obtain the correlation curve. The size distributions based on intensity diffusion were obtained using the general-purpose model in the standard Malvern software. To study the colloidal stabilization of CaP particles formed in the presence of Mono-CGMP or Poly-CGMP, two types of experiments were carried out without enzyme. In the first series, the concentration of the Poly-CGMP stock solution was fixed at 10 $g \cdot L^{-1}$ in a 50 mM Na-PB solution and the CaP particles were formed by one-pot precipitation by adding appropriate amounts of $CaCl_2$ to reach a final concentration of 10, 50, or 100 mM, respectively. Then, the solution was rapidly transferred into the DLS instrument for analysis. The delay between the addition of $CaCl_2$ and the start of analysis was one minute. In the second series of experiments, only Poly-CGMP solutions were

prepared between 1 and 20 $g{\cdot}L^{-1}$ in a 100 mM Na-PB solution. The CaP particles were precipitated by adding a fixed amount of 2 µL $CaCl_2$ (5M), e.g. 10 mM Ca^{2+} as final concentration, to 1 mL of Poly-CGMP in Na-PB. The solution was kept at rest for 30 minutes at 25 °C, before the DLS measurements. The average and standard deviation were calculated from the data obtained from three replicates.

2.6 ^{1}H and ^{31}P solid-state NMR

The experiments were performed on a Bruker Biospin Avance III spectrometer, at a magnetic field of 7 T corresponding to a ^{1}H resonance frequency of 300 MHz, using a 4 mm probe. The spinning frequency was set to 12.5 kHz, unless otherwise stated. A 300 s recycle delay was used for ^{31}P direct excitation spectra (single-pulse experiments). Proton to phosphorus cross-polarization (CP) 1D spectra were recorded with ^{1}H and ^{31}P resonance frequency fields of 47 and 34 kHz respectively, using a contact time of 1 ms. In two-dimensional ^{1}H-^{31}P HETCOR correlations, proton to phosphorus-31 polarization transfer was achieved by CP with a 2 ms contact time. SPINAL-64 proton decoupling at 60 kHz was applied during 40 ms ^{31}P acquisition. ^{31}P and ^{1}H chemical shifts are relative to external 85% H_3PO_4 and TMS standards. Deconvolution and low spinning frequency spectra simulations were performed with dmfit software [25,26].

3. Results and discussion

3.1 CaP-based Biocatalyst Morphology

The main goal of this study was to investigate the formation of calcium phosphate-supported biocatalysts for food applications. For this purpose, organic phosphate sources (CGMP), namely phosphopeptides, were used to produce hybrid materials previously labelled CaP,

CaP-Enz, CaP-Enz-Mono and CaP-Enz-Poly. Figures 1 and SI5 show the morphologies of the aforementioned systems (CaP, CaP-Enz, CaP-Enz-Mono and CaP-Enz-Poly), as obtained by scanning electron microscopy. Both pure CaP and CaP-Enz particles had platelets of brushite-like shape, which suggests that the enzyme has no influence on the formation of CaP particles (Figure 1a, 1b and Figure SI5). On the contrary, the addition of phosphopeptides significantly influenced the morphology of the resulting hybrid particles. Indeed, the platelets size decreased when using monomeric CGMP (Figure 1c) to completely disappear when using polymeric CGMP (Figure 1d). Moreover, aggregated, almost spherical nanoparticles appeared in the samples CaP-Enz-Mono and CaP-Enz-Poly. The sphericity of the particles seems to be better defined in the presence of the polymer compound and the size of the primary particles is around 50 – 100 nm, which is close to the R_h of the pure polyglycopeptide in aqueous solution [27].

3.2 CaP particles formation followed by DLS

To decipher the formation of CaP particles, dynamic light scattering (DLS) analysis was performed in the presence of Mono-CGMP and Poly-CGMP to evidence their influence in the colloidal stabilization of CaP particles. As the synthesis is performed at pH 7 in the presence of Na_2HPO_4 as reagent, the precipitation of brushite ($CaHPO_4{\cdot}2H_2O$) should be the most favourable solubility product constant (K_{sp}, of $2.6x10^{-7}$ M^2). In the conditions chosen for DLS experiments, the ion activity product ($[Ca^{2+}]x[HPO_4^-]$) is high and therefore the supersaturation might explain the rapid precipitation of CaP at room temperature (20 °C). According to the DLS data (not shown), the pure CaP particles rapidly grew (within minutes) to a size larger than 1 µm and subsequently settled down under the influence of gravity. The

same behaviour was observed for the CaP-Enz matrix, indicating that lactase does not act as a stabilizer either. In that case, the electrostatic repulsions from the surface charge are not high enough to prevent particle growth to large dimensions. In the case of Mono-CGMP and Poly-CGMP, different kinetics were observed. Figure 2a depicts the variation of the hydrodynamic radius (R_h) during the formation of CaP particles over time, at three different concentrations of Ca^{2+} ions, i.e., 10, 50 and 100 mM, in the presence of Poly-CGMP at a concentration of 10 $g \cdot L^{-1}$.

In the presence of Mono-CGMP (data not shown), the formation rate of CaP particles is slightly slowed down compared to pure CaP or CaP-Enz particles, which formed instantaneously. The monomeric CGMP does not seem to be an efficient particle growth inhibitor or colloidal stabilizer because large CaP particles (> 500 and 1000 nm) were formed within around 10 minutes in the presence of 10, 50 and 100 mM of Ca^{2+}. Then, at longer time scales (> 10 min), a settlement phenomenon appeared. However, under the same conditions, CaP particles formation was found to be significantly delayed in the presence of the polyglycopeptide (Figure 2a). In fact, looking at the R_h values extracted from scattering intensity over time, below 10 minutes, the radius of the scattering objects has a size between 60 and 75 nm (corresponding to the P1 plateau), which corresponds to the R_h of the polyglycopeptide [27]. Then, suddenly, a new plateau of size around 90 – 110 nm was reached (referred to as the P2 plateau) for any concentration of Ca^{2+}. According to the representations of the intensity size distribution data (Figure 2b, 2c), the CaP clusters are stabilized by the polymeric CGMP, leading to highly monodisperse nanoparticles. This indicates that the Poly-CGMP provides much greater colloidal stability to the CaP particles than its monomeric form. Moreover, the size distribution representation for the P1 plateau overlaps the size range of the P2 plateau distribution. This could be related to ripening,

254 which is a continuous process along the reaction time. Thus, the particle size distribution
255 measured at a given time must comprise particles from both the initial stage and the
256 ripened stage. These results obtained on the CaP and Poly-CGMP system seem to be similar
257 to those observed in the case of CaP particles stabilized by Fetuin-A. Indeed, Fetuin-A is
258 known to be an inhibitor of CaP mineralization and deposition in the soft tissues of animals
259 and humans [28].
260 Wald *et al.* [28] found that in the presence of Fetuin-A, the CaP/Fetuin-A particles formed
261 had initially a R_h of 40 – 60 nm which ripened to a R_h of around 100 nm after a lag period of
262 about 300 minutes. They also argued that particle size was mainly governed by the
263 concentrations of the mineral ion and Fetuin-A. Increasing the concentration of Fetuin-A led
264 to smaller particles, while increasing the concentration of the mineral ion accelerated the
265 particle ripening process at fixed amount of Fetuin-A. Thus, they proposed that the size and
266 stability of the 'calciprotein' particles could be controlled by a combination of these
267 physicochemical parameters. It should be noted that Fetuin-A has several phosphoserine
268 residues and O- and N-glycosylated chemical groups (see *e.g.* P02765 in www.uniprot.org).
269 In our case, the monomeric CGMP prepared from κ-casein phosphorylated serine residues
270 and the polyglycopeptide synthesized from the monomeric form is a polyelectrolyte.
271 Therefore, it has a higher density of phosphoserines per molecule, which allows binding to
272 the surface of inorganic CaP in a way analogous to caseins micelles for CaP nanoclusters
273 [29]. Moreover, by analogy with Fetuin-A, the polymeric CGMP also has O-glycosylated
274 residues, which are known to control the size and stability of CaP particles by varying the
275 Poly-CGMP concentration, as presented in Figure 3. Thus, according to Figure 3, the R_H
276 values (measured after 10 min of reaction) decrease with increasing Poly-CGMP amount in
277 the solution. Then, above 10 $g \cdot L^{-1}$, the CaP particle size is stabilized at a hydrodynamic radius

of around 100 nm. This clearly demonstrates that the polymeric CGMP acts as a colloidal stabilizer, and it can be speculated that the mode of action is a combination of electrostatic and steric repulsions originating from a combination of a charged backbone and a higher molar mass of the polyelectrolyte. The threshold of 10 $g \cdot L^{-1}$ can be designated as the maximum surface concentration of the polymer adsorbed on the CaP particles formed.

3.3 Textural and structural properties

Nitrogen adsorption isotherms have led to a better understanding of the textural properties of the dried materials (see SI4 Table and Figures). The results show that the specific area (A_{BET}) and the mesoporous volume (V_{mes}) increased in the case of CaP-Enz-Mono and CaP-Enz-Poly particles compared to CaP and CaP-Enz: 70 and 59 $m^2 \cdot g^{-1}$ vs 36 and 31 $m^2 \cdot g^{-1}$ for A_{BET}, respectively, and 0.218 vs 0.150 $cm^3 \cdot g^{-1}$ in average, for V_{mes}, respectively. This could be due to voids formed between aggregated nanoparticles or, in other words, due to interparticle porosity. In the case of platelet-shaped particles, these voids are almost negligible at the mesoscale. On the contrary, less ordered aggregated nanoparticles, trapped in an organic network, might induce the observed mesoporosity (Table SI4). Furthermore, the pore size distribution (PSD) became much more monodisperse in the presence of Mono-CGMP or Poly-CGMP, and it was centred on 15 nm (Figure SI4 a, b). These results highlight the fact that the porous texture in the mesopore range (2-50 nm) of the inorganic carrier matrix can be tailored by the monomer or the polymer to obtain pore sizes suitable for enzyme entrapment (herein Ha-Lactase, 14 nm in size). In order to understand whether the CGMP (monomer or polymer) interferes with the inorganic particles in the crystallisation process, the variation of crystallinity in the CaP, CaP-Enz, CaP-Enz-Mono and CaP-Enz-Poly samples was measured by XRD (See 4a,b). Thus, the platelet-shaped particles observed for the CaP or CaP-Enz systems

were clearly identified as monoclinic, prismatic crystals of brushite ($CaHPO_4 \cdot 2H_2O$). This result agrees with the existing literature. For instance, under neutral or slightly acidic conditions, wet precipitation of CaP particles leads to the rapid formation of a platelet-like brushite phase (see Fig. 4a) [2]. The intensity and resolution of the crystal peaks corresponding to brushite significantly decreased in the case of CaP-Enz-Poly. The broadened pattern obtained for CaP-Enz-Poly is a typical signature of a more disordered calcium phosphate phase such as reported by Sun et al. [30].

However, the most pronounced crystal peaks still present in the signal of the CaP-Enz-Poly sample mainly fitted the hydroxyapatite (Hap) crystalline form ($Ca_{10-x}(PO_4)_{6-x}(HPO_4)_x(OH)_{2-x}$) (see Fig4b). Finally, the ratio between the areas under the broadened bands and the sharp peaks gave an estimate of the degree of disorder in each sample prepared. Thus, it appears that the proportion of disordered phase in the CaP particles increased from 15% without CGMP to around 45 % in the presence of the phosphopeptide [7]. This clearly indicates that polymeric CGMP disturbed the crystallization process of CaP nanoparticles. Indications on the nature of phases can also be obtained from the Ca/P molar ratio determined by elemental analysis (see Table SI7). Indeed, it is known from the literature that the Ca/P molar ratio can vary between 1.5 and 1.67 for Hap and calcium-depleted Hap, while it is 1 for brushite and varies from 1.2 to 2.2 for amorphous calcium phosphate, respectively [1,2]. A Ca/P molar ratio of 1.08 was determined in the case of CaP particles, thus confirming the presence of brushite, and of 1.27 in the case of CaP-Enz-Poly particles (1.25 for CaP-Mono), which could correspond to amorphous Hap (see SI7).

3.4 Solid-state NMR

Solid-state NMR (ssNMR) was used to further characterize the different types of phosphates and phosphorus environments in CaP, Cap-Enz, CaP-Enz-Mono and CaP-Enz-Poly. Direct ^{31}P excitation with a long recycle delay allows quantitative analysis of different phosphorus-containing species, whereas cross-polarization (CP) experiments enhance the ^{31}P signals of near-proton and immobilized phosphorus atoms, as shown in Figure 5. ^{31}P chemical shifts as well as the relative signal intensity in the two types of 1D spectra enabled a first identification of different phosphorus species.

Additional information was obtained by recording the ^{31}P low spinning frequency spectra and simulating these spectra with different anisotropy parameters. The experimental details and simulations are given in SI8. The 1D ^{31}P spectra of CaP, CaP-Enz, CaP-Enz-Mono and CaP-Enz-Poly samples (Figure 5) exhibit two major peaks at 3-3.3 ppm and 1.5 ppm. An additional signal around -0.2 ppm is also present, excepted for CaP.

The component at 1.5 ppm corresponds to protonated phosphates according to chemical shifts reported in the literature. Its protonation state is confirmed by the high relative intensity in the CP spectra. Its contribution is similar in CaP and CaP-Enz, 56% and 51%, respectively, but largely decreases in the presence of mono- or poly-CGMP (see Tables SI8-1, SI8-2, Fig. SI8-1 and Fig.SI8-2). CaP, CaP-Enz, CaP-Mono spinning sidebands manifolds in 1D ^{31}P low spinning frequency CP spectra, can be simulated using δ_{aniso} and η values of 62 ppm and 0.8, respectively (see Fig. SI8-3 and Tab. SI8-3). These parameters are typical for brushite [31-33]. The broader signal of CaP-Enz-Poly is more difficult to deconvolute but gives an δ_{aniso} value around 45 ppm and is therefore probably not related to brushite (SI8-4). These observations are consistent with the XRD data. Confirmation of brushite phase comes from 2D ^{1}H-^{31}P correlations: strong cross-signals between ^{31}P at 1.5 ppm and ^{1}H at 10.7 ppm in CaP-Enz are indeed typical for brushite (see SI8.5) [34,35]. The ^{31}P signal at 3-3.3 ppm is

broad (2 to 2.5 ppm FWHM) and its relative intensity is lower in CP spectra. The contribution of this peak to the total ^{31}P signal is 44% in CaP and CaP-Enz samples, and 65% in CaP-Enz-Mono and 67% in CaP-Enz-Poly samples (see Table SI8.1). Its anisotropy contribution is not visible in the low spinning frequency experiments of CaP and CaP-Enz, whereas in CaP-Mono and CaP-Enz-Mono it shows an anisotropy parameter around -20 or -30 ppm (see Figure SI8.4), consistent with inorganic colloidal calcium phosphate in a hydroxyapatite-like environment. In the 2D ^{1}H-^{31}P spectra of CaP-Enz-Poly, a correlation between the ^{31}P signal at 3-3.3 ppm and a ^{1}H hydroxyl group resonance at -0.2 ppm is again a hallmark of hydroxyapatite [26,31,36]. This correlation is more intense in CaP-Enz-Poly, in agreement with XRD data indicating a hydroxyapatite phase representing 96% of the crystalline phase (data from area integration of crystal peaks, not shown). The C-terminal peptide of κ-casein is flexible and is known to remain a flexible tail in casein micelles, in contrast to α- and β-caseins, which participate in micelle formation and show an immobilized phosphoserine (SerP) ^{31}P signal [35]. Therefore, monomeric CGMP should not interact extensively with calcium phosphate particles. The ^{31}P data of CaP-Mono and CaP-Enz-Mono (brushite signal, only a small amount of Hap-like particles) are closer to CaP and CaP-Enz than to CaP-Enz-Poly. On the contrary, the CaP-Enz-Poly sample exhibits a higher proportion of Hap-like phosphate. The broad ^{31}P signal of CaP-Enz-Poly around 1.8-2 ppm present in 1D CP spectra (left peak, Figure 5) and in 2D HETCOR (SI8-5) correlation can be tentatively assigned to immobilized phosphoserine from poly-CGMP [35]. The immobilization of these SerP groups could be ascribed to their participation in the interaction with calcium phosphate particles [35]. Peptide immobilization, and thus SerP participation in colloid formation, seems only observable in the presence of polymeric CGMP.

The detailed characterization of the inorganic particle seems to indicate that the presence of peptide leads to less crystalline particles (XRD) and to the appearance of hydroxyapatite-like calcium phosphates (XRD and NMR). The immobilization of the peptide phosphoserine groups by participation in the interaction with the calcium phosphate particles has been tentatively evidenced by NMR only for CaP-Enz-Poly. The phosphoglycopeptide polymer appears to be necessary to allow enzyme retention with good activity, to increase the proportion of hydroxyapatite-like particle and to prevent the formation of the brushite phase.

3.5 Enzyme activity of the Hap-like catalytic supports

The Figure 6 compares for the different samples: i- the amount of lactase immobilized in the different samples prepared by in situ wet precipitation as described above, and ii- the respective catalytic activities. Thus, the CaP-Enz and CaP-Enz-Mono particles contained respectively 52 ± 19 and 34 ± 21 mg of immobilized lactase per g of dry powder, while the CaP-Enz-Poly particles had an amount of encapsulated lactase of 125 ± 4 $mg \cdot g^{-1}$, which is more than twice the amount immobilized in the CaP-Enz and CaP-Enz-Mono matrices. The amount of enzyme immobilized in CaP-Enz and CaP-Enz-Mono particles is of the same order of magnitude as that typically observed for silica matrix (10 – 70 $mg \cdot g^{-1}$) [9]. In addition, according to the standard deviation values, the lactase encapsulation process seems to be highly reproducible in the case of CaP-Enz-Poly particles compared to the other two samples.

Consequently, the supported enzyme presented variable catalytic performance, as also shown in Figure 6. It can be seen that the activity of the CaP-Enz-Mono sample is about three times higher than that of the CaP-Enz sample, despite the similar amounts of

395 immobilized protein. However, the activity of the CaP-Enz-Poly sample was found to be
396 almost 10 times higher than that of the CaP-Enz material. The average specific activity was
397 found to be 1060, 4811 and 4843 NLU·g^{-1} of protein for CaP-Enz, CaP-Enz-Mono and CaP-
398 Enz-Poly samples, respectively. The specific activity of the immobilized enzyme in the CaP-
399 Enz sample was found to be around 100 times lower than that of the free enzyme (100
400 kNLU·g^{-1} of protein), while it was only 20 times lower in the case of CaP-Enz- Mono and CaP-
401 Enz-Poly samples. A comparison of the specific activity of immobilized and free enzyme
402 phenomenologically indicates the hindrance to activity due to slower mass transport of the
403 substrate and product through the inorganic matrix. This suggests significant resistance to
404 mass transfer (diffusion) through the particles. The narrowest PSD found for the CaP-Enz-
405 Poly particles could explain the better retention and the higher activity of enzyme in CaP-
406 Enz-Poly particles compared to the other two types of particles. The differences in
407 enzymatic activity between the materials CaP-Enz, CaP-Enz-Mono and CaP-Enz-Poly might
408 be due to some differences of particles mesoporosity as well as to enzyme denaturation
409 caused by adsorption on the inorganic matrix surface. Indeed, a direct interaction of the
410 enzyme with the surface of pure CaP might lead to a partial denaturation of the enzyme,
411 e.g. due to some changes in the quaternary/tertiary structure. A specific activity about five
412 times higher for CaP-Enz-Mono and CaP-Enz-Poly than for CaP-Enz particles indicates some
413 protective effect in the case of monomeric and polymeric CGMP. However, CaP-Enz-Poly
414 had a much higher total activity (607 ± 34 NLU.g^{-1} of dry powder) than monomeric CGMP-
415 coated particles (161 ± 70 NLU.g^{-1} of dry powder), which indicates that the difference
416 between the activities of these two types of particles is mainly caused by the different
417 amounts of encapsulated enzyme (Figure 6). This suggests that the monomer or polymer
418 preferentially adsorbs on the CaP surface and that the enzyme is therefore mainly trapped

419 in the organic network where the quaternary/tertiary structure of the lactase might be
420 better preserved. Similar observations were made on lactase immobilized in silica matrix,
421 where the enzyme encapsulated in macropores was found to be more active than the
422 enzyme adsorbed in mesopores [4]. The authors proposed that the difference in activity was
423 related to the quaternary structure of lactase (monomers vs dimers or tetramers).

424 ## 4. Conclusion

425 In conclusion, through the careful selection of precipitation conditions, phosphopolypeptide
426 polymers have been found to be efficient controllers of crystal growth, crystallinity and
427 colloidal stability of calcium phosphate particles (CaP) when produced by a wet precipitation
428 method. Changes in the crystalline phase, from brushite to hydroxyapatite, crystal size and
429 disorder led to changes in the mesoporous texture of these particles and made them
430 suitable for trapping small bioactive macromolecules such as enzymes while preventing
431 significant loss of catalytic activity. The polymeric form was found to be more suitable for
432 encapsulation since it produces a good interaction with the CaP surface and imparts
433 excellent colloidal stability to the particles. Based on this mechanism, it can be concluded
434 that any bio-macromolecule with organic phosphates and flexible structure can be used to
435 modulate the mesoporosity of calcium-based inorganic particles. The underlying
436 fundamental mechanism seems to be the ionic interactions between the charged
437 macromolecule and the charged inorganic surface. Thus, extending the proposal further,
438 any (bio)macromolecule with strong ionic groups present in its chain that can ionically
439 interact with an inorganic surface should modify its mesoporous texture. Of course, there
440 could be variations originating from other parameters such as the flexibility of the chain, the
441 distribution of charged groups and the presence of other groups that interact with the

surface via other types of weak interactions. Using biopolymers for controlling/modulating the mesoporous texture of inorganic matrices seems to be a viable option for practical applications. Modified mesoporosity with a suitable pore size can be also used for the immobilization of various bioactive molecules, macromolecules or cells targeting straightforward applications for food packaging, (ref https://doi.org/10.3390/polym13234198) pharmaceutics (ref notre Adv Colloids and Interface science) or functional food (ref https://doi.org/10.1111/1541-4337.13049).

Conflicts of interest

There are no conflicts to declare.

Funding

This work was supported by the People Programme (Marie Curie Actions) of the European Union's Seventh Framework Programme FP7/2007-2013/ under REA (grant agreement n° 606713). A.C and A.P. acknowledge financial support from the "Impact Biomolecules" project of the "Lorraine Université d'Excellence" (Investissements d'avenir – ANR 15-004).

Acknowledgements

SKD *et al* would like to thank Mr. Jean Cauzid for SEM analysis and Mr. Jérôme Marin for elemental analysis measurements.

References

[1] S. Schweizer, A. Taubert, Macromol. Biosci., 2007, 7, 1085. https://doi.org/10.1002/mabi.200600283

[2] K. Lin, C. Wu, J. Chang, Acta Biomaterialia, 2014, 10, 4071. https://doi.org/10.1016/j.actbio.2014.06.017

[3] I.-A. Pavel, S.F. Prazeres, G. Montalvo, C. Garcia Ruiz, V. Nicolas, A. Celzard, F. Dehez, L. Canabady-Rochelle, N. Canilho, A. Pasc, Langmuir, 2017, 33, 3333. https://doi.org/10.1021/acs.langmuir.7b00134

[4] I.-A. Pavel, M. Girardon, S. El Hajj, S. Parant, F. Amadei, S. Kaufmann, M. Tanaka, V. Fierro, A. Celzard, N. Canilho, A. Pasc, J Mater Chem B, 2018, 6, 5633. https://doi.org/10.1039/C8TB01114A

[5] Hou, N. Ghéczy, D. Messmer, K. Szymańska, J. Adamcik, R. Mezzenga, A.B. Jarzębski, P. Walde, ACS Omega, 2019, 4, 7795. https://doi.org/10.1021/acsomega.9b00286

[6] K.J. Cross, N.L. Huq, J.E. Palamara, J.W. Perich, E.C. Reynolds, J. Biol. Chem., 2005, 280, 15362. https://doi.org/10.1074/jbc.M413504200

[7] C. Combes, C. Rey, Acta Biomaterialia, 2010, 6, 3362. https://doi.org/10.1016/j.actbio.2010.02.017

[8] C. Holt, J.A. Carver, H. Ecroyd, D.C. Thorn, J Dairy Sci., 2013, 96, 1. https://doi.org/10.3168/jds.2013-6831

[9] Pierre, A. C. Biocatal. Biotransformation, 2004, 22, 145. https://doi.org/10.1080/10242420412331283314

[10] B. Dziuba, M. Dziuba, Acta Scientiarum Polonorum, Technologia Alimentaria, 2014, 13, 5.

[11] M.J. Martinez, V.M. Pizones Ruiz-Henestrosa, C. Carrera Sánchez, J.M. Rodríguez Patino, A.M.R. Pilosof, Colloids Surf. B, 2012, 95, 214. http://hdl.handle.net/20.500.12110/paper_09277765_v95_n_p214_Martinez

[12] R. Morales, M.J. Martinez, A.M.R. Pilosof, International Dairy Journal, 2015, 49, 30. https://doi.org/10.1016/j.idairyj.2015.04.006

[13] R. Silva Diniz, J.S. dos Reis Coimbra, A.V.N. de Carvalho Teixeira, A. Ribeiro da Costa, I.J. Boggione Santos, G. Costa Bressan, A.M. da Cruz Rodrigues, L.H. Meller da Silva, Food Research International, 2014, 64, 157. https://doi.org/10.1016/j.foodres.2014.05.079

[14] A. Tolkach, U. Kulozik, J. Food Eng., 2005, 67, 13. https://doi.org/10.1016/j.jfoodeng.2004.05.058

[15] C. Thomä-Worringer, J. Sørensen, R. López-Fandiño, International Dairy Journal, 2006, 16, 1324. https://doi.org/10.1016/j.idairyj.2006.06.012

[16] M.E. Farías, M.J. Martinez, A.M.R. Pilosof, International Dairy Journal, 2010, 20, 79. https://doi.org/10.1016/j.idairyj.2009.09.002

[17] E. Rojas, G. Torres, Food Science and Technology, 2013, 33, 14. https://doi.org/10.1590/S0101-20612013005000027

[18] V. Narwal, N. Sharma, R. Sharma, Y.S. Rajput, B. Mann, International Journal of Dairy Technology, 2017, 70, 1. https://doi.org/10.1111/1471-0307.12452

[19] S.H. Kim, K.P. Lim, H.S. Kim, J. Dairy Sci., 1997, 80, 2264. https://doi.org/10.3168/jds.S0022-0302(97)76175-7

501 [20] J.E. Folk, P.W. Cole, Biochim. Biophys. Acta, 1966, 122, 244.
502 https://doi.org/10.1016/0926-6593(66)90066-X

503 [21] S. Brunauer, P.H. Emmet, E. Teller, J. Am. Chem. Soc., 1938, 309.
504 https://doi.org/10.1021/ja01269a023

505 [22] M.M. Dubinin, 1989, Carbon 27, 457. https://doi.org/10.1016/0008-6223(89)90078-X

506 [23] M. Kruk, M. Jaroniec and M. Sayari, Langmuir, 1997, 13, 6267.
507 https://doi.org/10.1021/la970776m

508 [24] P. Barret, L. G. Joyner and P. P. Halenda, J. Am. Chem. Soc., 1951, 73, 373.
509 https://doi.org/10.1021/ja01145a126

510 [25] D. Massiot, F. Fayon, M. Capron, I. King, S. Le Calvé, B. Alonso, J. O. Durand, B. Bujoli, Z.
511 H. Gan and G. Hoatson, Magn. Reson. Chem., 2002, 40, 70. https://doi.org/10.1002/mrc.984

512 [26] W.P. Rothwell, J.S. Waugh, J.P. Yesinowski, J. Am. Chem. Soc., 1980, 102, 2637.
513 https://doi.org/10.1021/ja00528a020

514 [27] International Patent Number W02018/134066 Al.

515 [28] J. Wald, S. Wiese, T. Eckert, W. Jahnen-Dechent, W. Richtering, A. Heiss, Soft Matter,
516 2011, 7, 2869. https://doi.org/10.1039/C0SM01191F

517 [29] C.G. de Kruif, T. Huppertz, V.S. Urban, A.V. Petukhov, Adv. Colloid Interface Sci., 2012, 36,
518 171. https://doi.org/10.1016/j.cis.2012.01.002

519 [30] L. Sun, L.C. Chow, S.A. Frukhtbeyn, J.E. Bonevich, J Res Natl Inst Stand Technol. 2010, 115
520 (4), 243. https://doi.org/10.6028/jres.115.018

[31] M. Bak, J.K. Thomsen, H.J. Jakobsen, S.E. Petersen, T.E. Petersen, N. C. Nielsen, J Urol., 2000, 164, 856. https://doi.org/10.1097/00005392-200009010-00062

[32] Z. Hinedi, S. Goldberg, A. Chang, J. Yesinowski, J. Colloid Interface Sci., 1992, 152, 141. https://doi.org/10.1016/0021-9797(92)90015-E

[33] J.P. Yesinowski, H. Eckert, J. Am. Chem. Soc. 1987, 109, 6274. https://doi.org/10.1021/ja00255a009

[34] R. Mathew, P.N. Gunawidjaja, I. Izquierdo-Barba, K. Jansson, A. García, D. Arcos, M. Vallet-Regí, M. Edén, J. Phys. Chem. C, 2011, 115, 20572. https://doi.org/10.1021/jp206237n

[35] J.K. Thomsen, H.J. Jakobsen, N.C. Nielsen, T.E. Petersen, L.K. Rasmussen, Eur. J. Biochem., 1995, 230, 454. https://doi.org/10.1111/j.1432-1033.1995.0454h.x

[36] M. Bak, L.K. Rasmussen, T.E. Petersen, N.C. Nielsen, J. Dairy Sci., 2001, 84, 1310. https://doi.org/10.3168/jds.S0022-0302(01)70160-9

[37] B. M. Fung, A. K. Khitrin and K. Ermolaev, J Magn Reson., 2000, 142, 97. https://doi.org/10.1006/jmre.1999.1896

Figure Captions

Figure 1. SEM images of dry particles showing platelets (a) CaP, (b) CaP-Enz, or nanoparticles (c) CaP-Enz-Mono and (d) CaP-Enz-Poly.

Figure 2. Mean hydrodynamic radius (R_H) of the CaP particles formed in the presence of Poly-CGMP: (a) R_H recorded over time; (b) size distribution recorded for P1 plateau; (c) size distribution recorded for P2 plateau. The Ca^{2+} concentrations in mM used for making the particles are shown in the legend.

Figure 3. Mean hydrodynamic radius (R_H) of the CaP particles formed in the presence of different bulk concentrations of Poly-CGMP, in 10 mM of Ca^{2+}.

Figure 4: XRD showing the presence of brushite in the CaP sample and the formation of highly amorphous structures in other samples, with predominance of hydroxyapatite.

Figure 5. 1D ^{31}P NMR spectra of CaP (black), CaP-Enz (blue), CaP-Enz-Mono (green) and CaP-Enz-Poly (red) (from bottom to top, respectively) at 12.5 kHz spinning frequency. Top signals: 1 ms CP ^{31}P spectra; Bottom signals: direct ^{31}P excitation. The vertical dashed lines, corresponding to different ^{31}P contributions as deconvoluted in Table SI8.1, are drawn to guide the eye. The dotted line corresponds to a putative fourth contribution observed only in CaP-Enz-Poly spectra, as shown in SI8.2.

Figure 6. Amount of immobilized lactase ($mg \cdot g^{-1}$ of material) and enzyme activity ($NLU \cdot g^{-1}$ of material) in the different types of matrix.

Figure 1

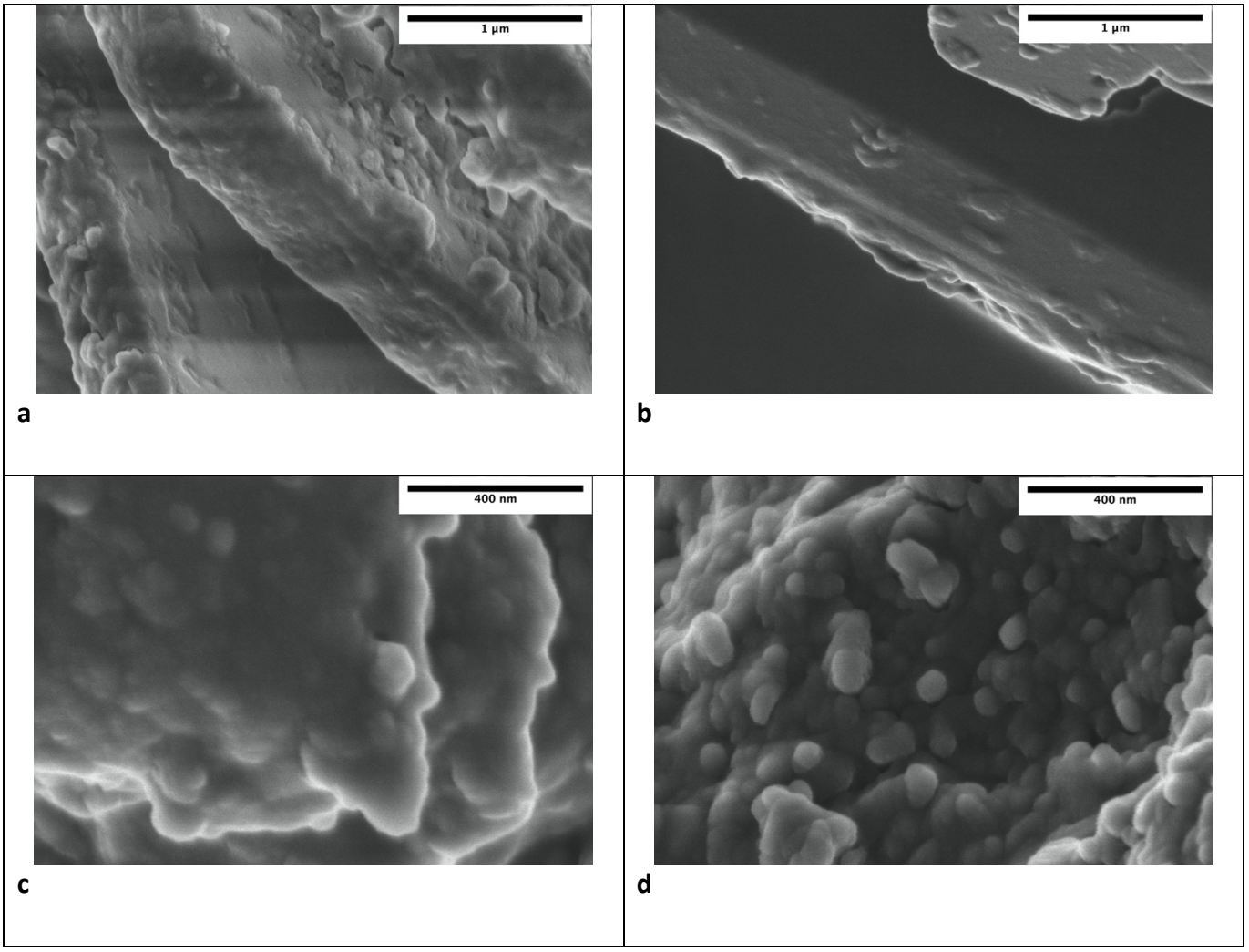

560 **Figure 2**

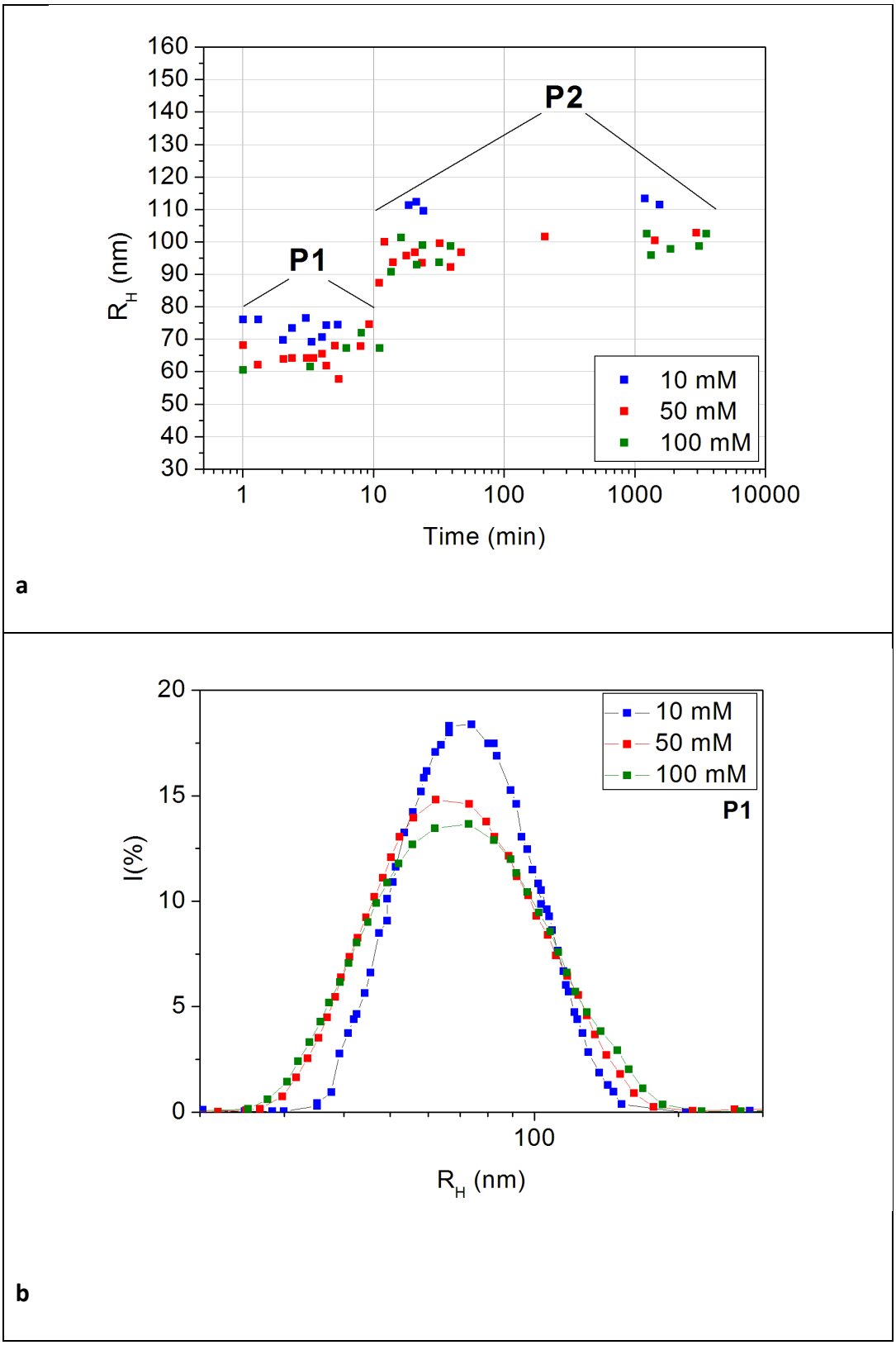
160
150
140
130
120
110
100
90
80
70
60
50
40
30
R_H (nm)
P1
P2
10 mM
50 mM
100 mM
1
10
100
1000
10000
Time (min)
a
20
15
10
5
0
I(%)
10 mM
50 mM
100 mM
P1
100
R_H (nm)
b

c

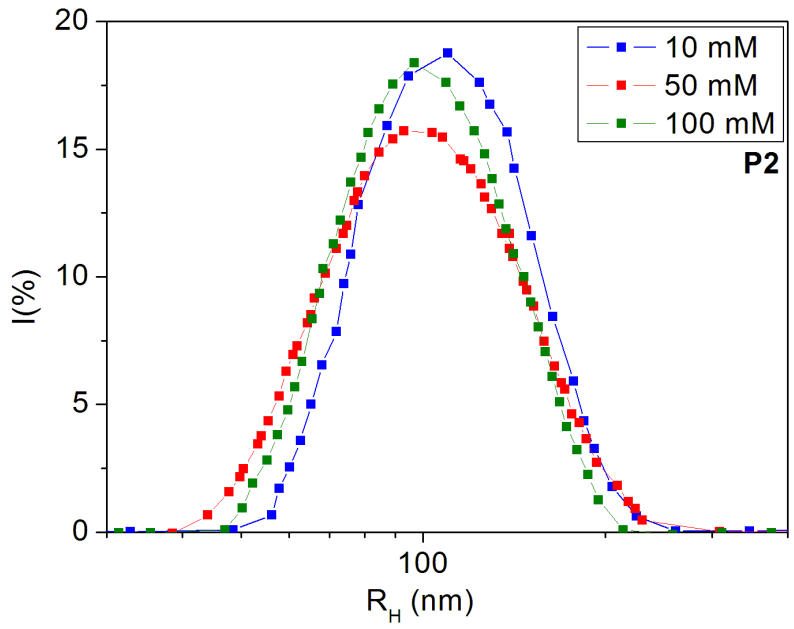

571

572

573 **Figure 3.**

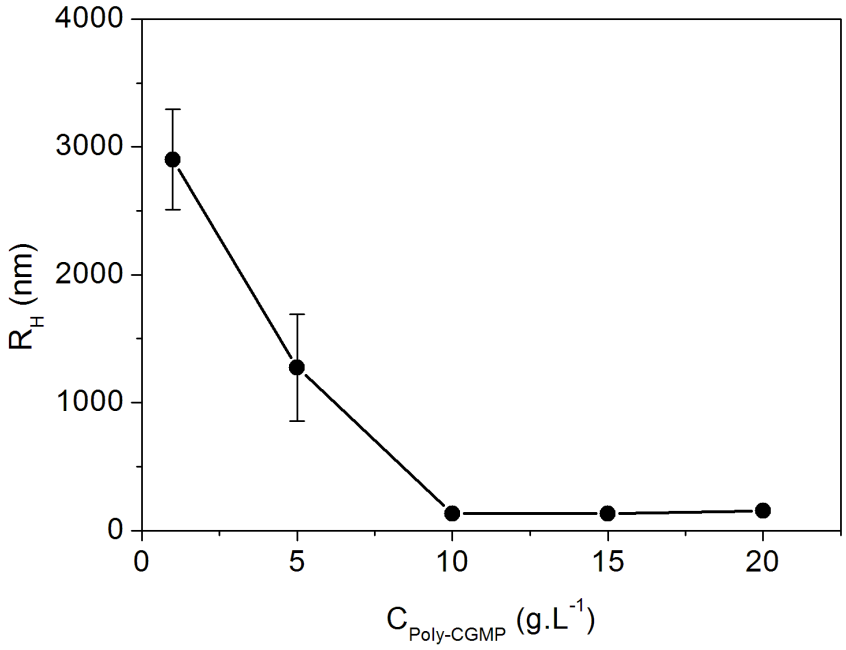

574

575

Figure 4.

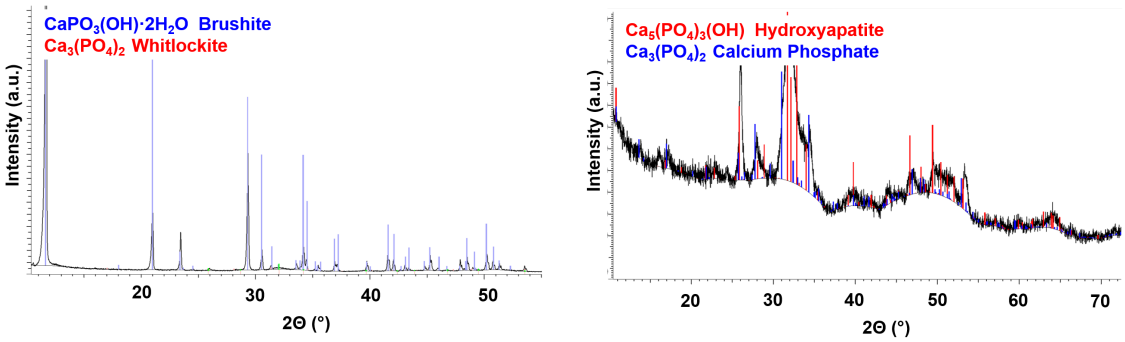
CaPO3(OH)·2H2O Brushite
Ca3(PO4)2 Whitlockite
Intensity (a.u.)
20
30
40
50
2Θ (°)
Ca5(PO4)3(OH) Hydroxyapatite
Ca3(PO4)2 Calcium Phosphate
Intensity (a.u.)
20
30
40
50
60
70
2Θ (°)

(a) **(b)**

580 **Figure 5.**

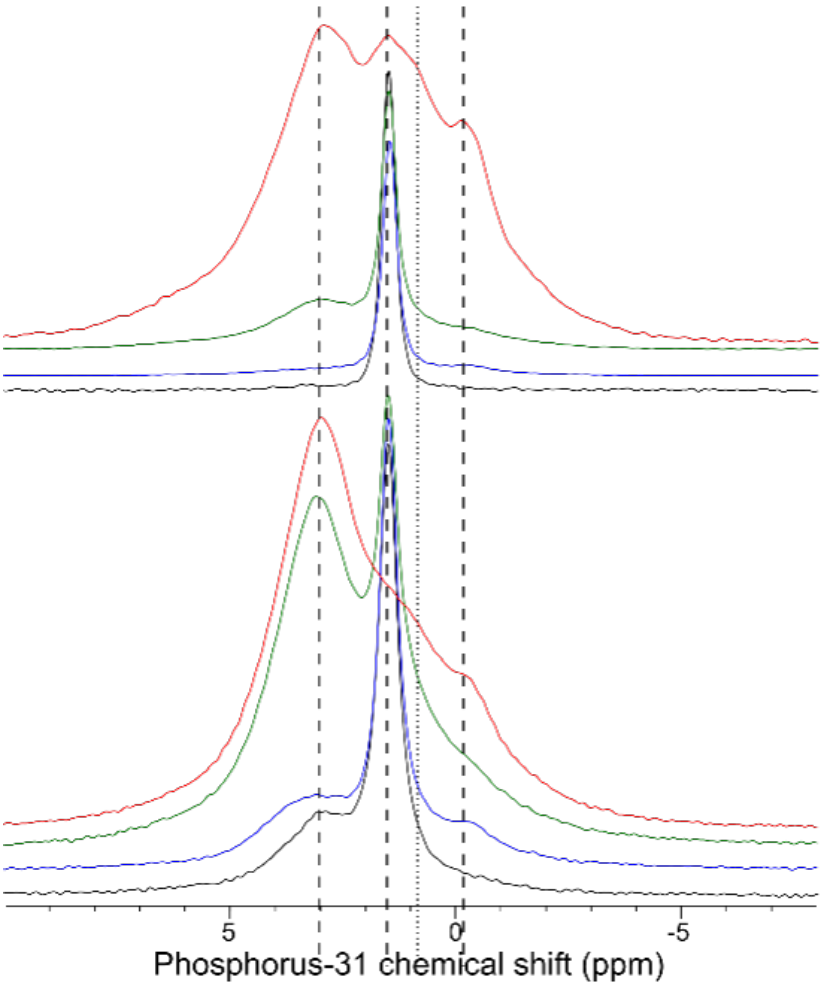

581

582

583 **Figure 6.**

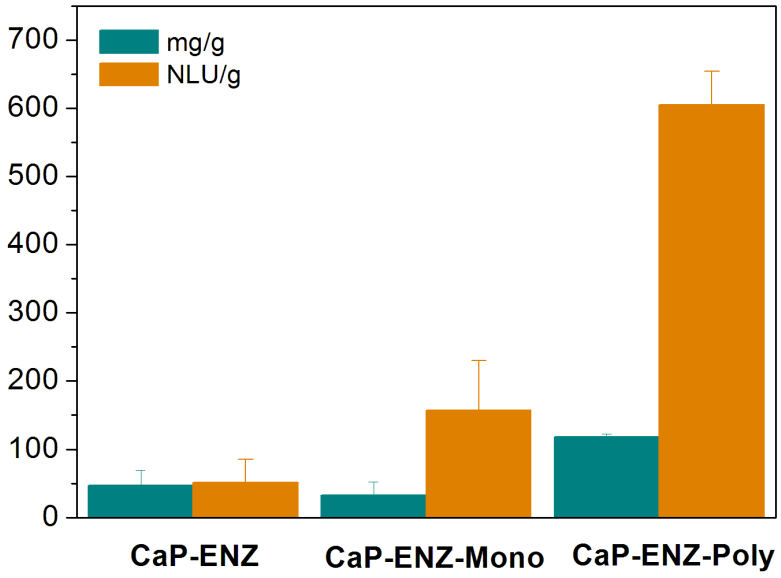

584

585